ChemPubSoc Europe

DOI: 10.1002/ejoc.201900171

EurJOC European Journal of Organic Chemistry

Full Paper

Catalysis Intermediates

The Intermediates in Lewis Acid Catalysis with Lanthanide Triflates

Guilherme L. Tripodi,[a] Thiago C. Correra,[b] Célio F. F. Angolini,[c] Bruno R. V. Ferreira,[d] Philippe Maître,[e] Marcos N. Eberlin,*[f,g] and Jana Roithová*[a]

Abstract: Lanthanide triflates are effective Lewis acid catalysts in reactions involving carbonyl compounds due to their high oxophilicity and water stability. Despite the growing interest, the identity of the catalytic species formed in lanthanide catalysed reactions is still unknown. We have therefore used mass spectrometry and ion spectroscopy to intercept and characterize the intermediates in a reaction catalysed by ytterbium and dysprosium triflates. We were able to identify a number of lanthanide intermediates formed in a simple condensation reaction between a C-acid and an aldehyde. Results show correlation between the reactivity of lanthanide complexes and their charge state and suggest that the triply charged complexes play a key role in lanthanide catalysed reactions. Spectroscopic data of the gaseous ions accompanied by theoretical calculations reveal that the difference between catalytic efficiencies of ytterbium and dysprosium ions can be explained by their different electrophilicity.

Introduction

Lewis acid catalysis enables and increases selectivity of many organic reactions under mild conditions.[1] Carbon–carbon and carbon–heteroatom bond-forming reactions can serve as examples.[2,3] These reactions are often based on Lewis-acid activation of a carbonyl group.[4]

[a] *Institute for Molecules and Materials, Radboud University, Heyendaalseweg 135, 6525 AJ Nijmegen, The Netherlands*
E-mail: jana.roithova@ru.nl
Guilherme.Tripodi@ru.nl
https://www.ru.nl/science/spectroscopy-and-catalysis/
[b] *Departament of Organic Chemistry, Institute of Chemistry, University of São Paulo, 05508–000, São Paulo-SP, Brazil*
E-mail: tcorrera@iq.usp.br
http://www.iq.usp.br/mcpl/
[c] *Center for Natural and Human Sciences, Federal University of ABC (UFABC), 09210–580, Santo André -SP, Brazil*
E-mail: celio.fernando@ufabc.edu.br
[d] *Instituto Federal do Norte de Minas Gerais Campus Salinas, 39560–000, Salinas-MG, Brazil*
E-mail: bruno.ferreira@ifnmg.edu.br
https://www.ifnmg.edu.br/salinas
[e] *Laboratoire de Chimie Physique, URM8000, CNRS, Univ. Paris-Sud, Université Paris-Saclay, 91405, Orsay, France*
E-mail: philippe.maitre@u-psud.fr
http://www.lcp.u-psud.fr/
[f] *ThoMSon Mass Spectrometry Laboratory, Institute of Chemistry, State University of Campinas, 13084–971, Campinas-SP, Brazil*
[g] *School of Engeneering, Mackenzie Presbiterian University, 01302907, São Paulo-SP, Brazil*
E-mail: mneberlin@gmail.com
Supporting information and ORCID(s) from the author(s) for this article are available on the WWW under https://doi.org/10.1002/ejoc.201900171.

The increasing popularity of lanthanides as Lewis acids stems from their stability at air and in water and their easy handling.[5,6] Lanthanides are strong Lewis acids therefore they have large affinities toward carbonyl oxygens. The Lewis-acid reactivity of lanthanide salts is particularly strong in combination with non-coordinating, electron-withdrawing anions such as triflates.[7] Examples of reactions catalysed by these metals include Friedel-Crafts acylations,[8] Michael additions,[9,10] aldol condensations[11] and cycloadditions.[12] They are also very useful as catalysts for multicomponent reactions[13–15] and in the synthesis of heterocycles,[16] and are widely embedded in the concept of asymmetric catalysis.[17]

The growing use and applications of lanthanides as catalysts calls for detailed understanding of their speciation in solution and their reactivity modes. As far as we know, there are no reports concerning the identity of the lanthanide intermediates formed in a reaction medium. Mass spectrometry (MS) is widely recognized as an effective tool to detect reactive species present in low concentrations such as transient reaction intermediates.[18,19,28,29,20–27] Electrospray ionization mass spectrometry (ESI-MS) is a highly sensitive technique for monitoring complex reaction mixtures.[30] Moreover, ESI-MS can be coupled to ion spectroscopy,[31–36] that can provide conclusive information about the structure of trapped ions in the gas phase. Here, we present a mechanistic study of a Lewis acid-catalysed Knoevenagel condensation between malonate, a typical C-acid, and an aldehyde (Scheme 1). We have applied a combination of tan-

Scheme 1. The lanthanide triflate catalysed Knoevenagel condensation reaction.

dem mass spectrometry and infrared multiphoton dissociation (IRMPD) spectroscopy[37] to intercept and characterize the lanthanide intermediates formed during the this reaction and also to investigate their reactivity.

Results and Discussion

Reaction Monitoring with ESI(+)-MS

For this mechanistic study, we chose ytterbium and dysprosium triflates as catalysts. Ytterbium has the largest Lewis acidity among lanthanides while dysprosium is known to have a high oxophilicity and is widely used in organic synthesis due to its lower cost.[38]

We have monitored the reaction between diethyl malonate (M) and benzaldehyde by sampling the reaction mixture at different reaction times (1µL aliquots of the reaction mixture were diluted in acetonitrile and directly infused into ESI(+)-MS).

Via ESI(+)-MS, several ions were "fished out" from the reaction solution. According to their exact mass and typical isotopic patterns, many lanthanide intermediates with different charges and ligands were assigned. All the molecular formulas were attributed with errors less than 1 ppm (Table S1 and S2). To exemplify, Figure 1 depicts the spectra acquired at t = 1 and 10 min for the ytterbium (up) and dysprosium (down) triflate catalysed reactions.

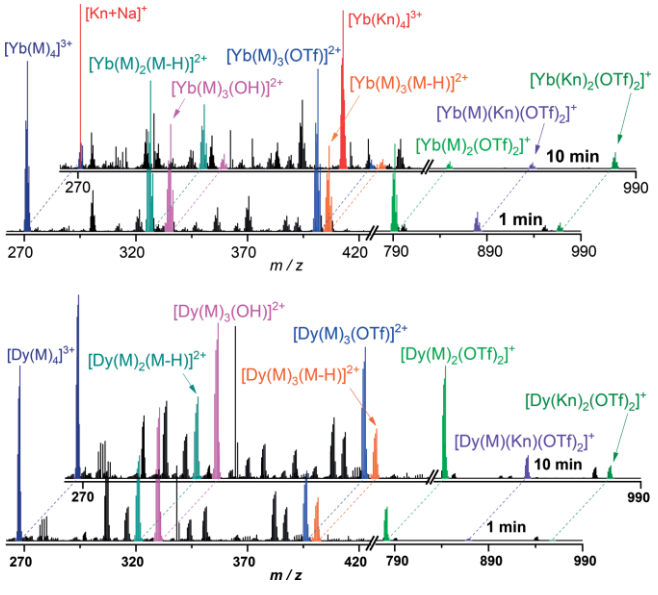

Figure 1. ESI(+)-MS for the sampling at t =1 and 10 min of the ytterbium (up) and dysprosium (down) triflate catalysed reaction between diethyl malonate and benzaldehyde. The ligands are depicted according to their initials: M for diethyl malonate, Kn for Knoevenagel adduct, and M-H for deprotonated diethyl malonate.

At t = 1 min, spectra for dysprosium and ytterbium exhibit the same profile, revealing the formation of the same type of lanthanide intermediates. Notably, however, samplings at later times reveal different kinetic information depending on the lanthanide. On one hand, for the ytterbium catalysed reaction, at t = 10 min the reactants are almost completely converted into the Knoevenagel product (Kn) which was trapped as a sodium adduct $[Kn + Na]^+$ whereas the most abundant lanthanide complex is $[Yb(Kn)_4]^{3+}$. On the other hand, the dysprosium catalysed reaction is considerably slower, hence the spectra at t = 1 min and t = 10 min have minimal differences and the dysprosium complex $[Dy(M)_4]^{3+}$ stays the most abundant ion in the spectra even after 10 minutes of the reaction time. The higher efficiency of the ytterbium catalyst was even more evidenced when we used a charge-tagged aldehyde instead of benzaldehyde (Figure S4).

Despite the complexity of the ESI(+)-MS spectra (Figure 1), insights into the step-by-step reaction mechanism could be derived from the evolution of the abundances of reaction intermediates. We observed all important lanthanide intermediates and, according to their charge and coordination number (N_{coord}), were able to classify them into three different mechanistic routes (Figure 2). Mechanistic route **A** proceeds via triply and doubly charged ytterbium complexes of N_{coord} = 8; route **B** proceeds via doubly and singly charged ytterbium complexes of N_{coord} = 7 and route **C** proceeds via singly charged and neutral ytterbium complexes of N_{coord} = 6. All three routes involve successive deprotonation and condensation steps.

Our ESI(+)-MS monitoring also provides qualitative information about kinetics associated with the different mechanistic routes. The triply charged complex $[Yb(M)_4]^{3+}$, which is the most abundant ion at t = 1 min, is almost completely consumed at t = 2 min by an α-hydrogen abstraction (Figure 2 – spectrum **A**). For the doubly charged complex $[Yb(M)_3(OTf)]^{2+}$, however, the α-hydrogen abstraction occurs with only 50 % conversion (spectrum **B**) from t = 1 to 2 min. The mechanistic route **C**, which contains singly charged/neutral ytterbium complexes, presented the lowest conversion of the malonates into the Knoevenagel adduct, that is evidenced by the high signal intensity of the complex $[Yb(M)_2(OTf)_2]^+$ still in t = 10 min. These different signal evolutions suggest that reaction is faster when proceeding within multiply charged lanthanide complexes. Hence, a higher charge state of the complex correlates with a higher reactivity of the coordinated malonate reactant.

To obtain more evidence for this charge/reactivity correlation of the lanthanide complexes, we took advantage of mass spectrometry capability to manipulate and isolate gaseous ions, and therefore investigate their individual reactivity towards a neutral reactant. Lanthanide intermediates with different charges were therefore reacted in the gas phase with benzaldehyde, their reactivities compared and finally correlated with their structures that were determined in the gas phase using IRMPD spectroscopy.

Gas Phase Experiments

Mass-selected lanthanide complexes reacted with benzaldehyde (0.1 mTorr) at zero collision energy.[39] Doubly and singly charged complexes $[Yb(M)_3(Tf)]^{2+}$ and $[Yb(M)_2(Tf)_2]^+$ reacted with benzaldehyde to yield an adduct (Figure 3A and Figure 3B). Most probably, this reaction corresponds to simple coordination of the aldehyde molecule to ytterbium. This attribution is consistent with the higher reactivity of $[Yb(M)_2(Tf)_2]^+$, which has a lower N_{coord} than $[Yb(M)_3(Tf)]^{2+}$. The smaller coordi-

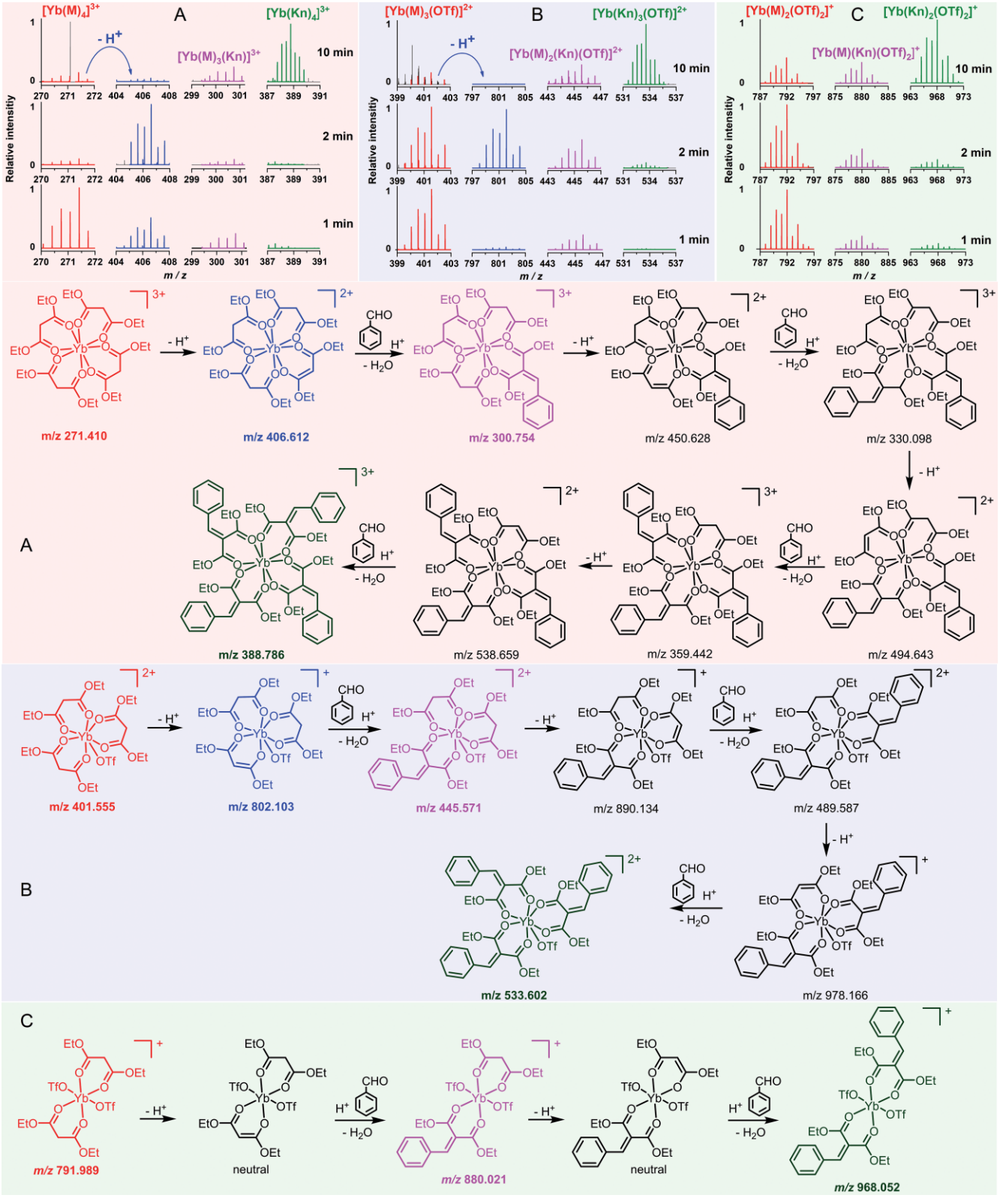

Figure 2. Selected views of the ESI(+)-MS for the sampling at t =1, 2 and 10 min of the ytterbium catalysed Knoevenagel condensation reaction chosen to highlight some of the ytterbium complexes presented in mechanistic routes **A**, **B** and **C**. The ytterbium complexes shown in the spectra are: the first complex of each mechanistic route (red), the complexes generated after the first deprotonation step (blue) and the first Knoevenagel condensation (pink), and the complex generated after the condensation of all the malonates (green).

nation number facilitates coordination of another molecule. The triply charged complex $[Yb(M)_4]^{3+}$ displays a different reactivity pattern (Figure 3C). The $[Yb(M)_4]^{3+}$ complex is deprotonated by benzaldehyde yielding the reactive enolate form of one of the

malonate ligands. Most probably, the high charge state increases the α-hydrogen acidity and thus enables the desired C-H activation by proton abstraction.

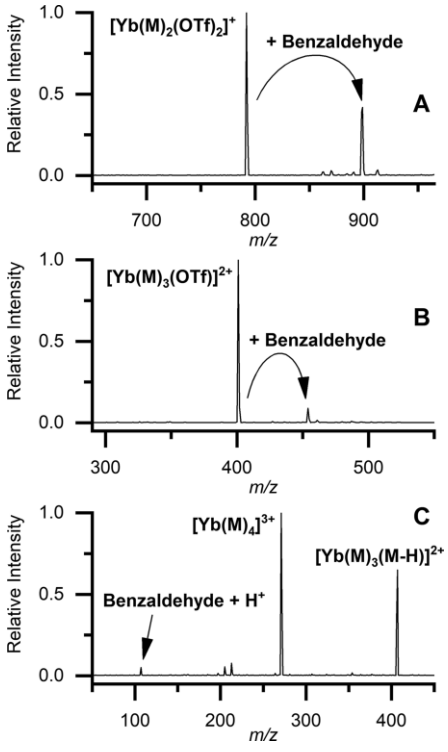

Figure 3. Product ion ESI(+)-MS/MS for the gas phase reactions of ytterbium complexes $[Yb(OTf)_2(M)_2]^+$ (A), $[Yb(OTf)(M)_3]^{2+}$ (B) and $[Yb(M)_4]^{3+}$ (C) at zero collision energy with 0.1 mTorr of benzaldehyde pressure.

DFT calculations show that exothermicity of the proton transfer between lanthanide complexes and benzaldehyde increases with increasing charge state of the complex (Scheme 2). While the reaction is endothermic for singly charged $[Yb(M)_2(Tf)_2]^+$, it becomes exothermic for $[Yb(M)_3(Tf)]^{2+}$ and $[Yb(M)_4]^{3+}$ as expected. We do not experimentally observe proton transfer between benzaldehyde and $[Yb(M)_3(Tf)]^{2+}$ because it is probably prevented by the Colomb barrier.[40]

IRMPD Spectra

In order to better understand the structure and reactivity differences between the complexes, we measured IRMPD spectra of the lanthanide complexes. The IRMPD spectra were recorded in the 900–1850 cm^{-1} range and compared to the theoretical vibrational spectra, which exhibited a good match with the experimental results (Figure 4). The analysis of the complexes geometry reveals that the ligands are organized around ytterbium in order to maximize the distance between themselves, as expected due to the low covalent character of the lanthanide-ligand bonds.[41]

In the 900–1500 cm^{-1} range of the IRMPD spectra for the complex $[Yb(M)_4]^{3+}$ we can observe many bands which, according to the DFT calculations, can be attributed mainly to C-H scissoring, wagging and twisting. For the complexes $[Yb(M)_3(Tf)]^{2+}$, $[Yb(M)_2(Tf)_2]^+$ and $[Dy(M)_2(Tf)_2]^+$ we can observe some additional stretching modes around 1000 cm^{-1} (S-O) and 1200 cm^{-1} (C-F), that overlaps with the previous described bands of the malonate ligands. All IRMPD spectra present an intense band at about 1670 cm^{-1}, which corresponds to the

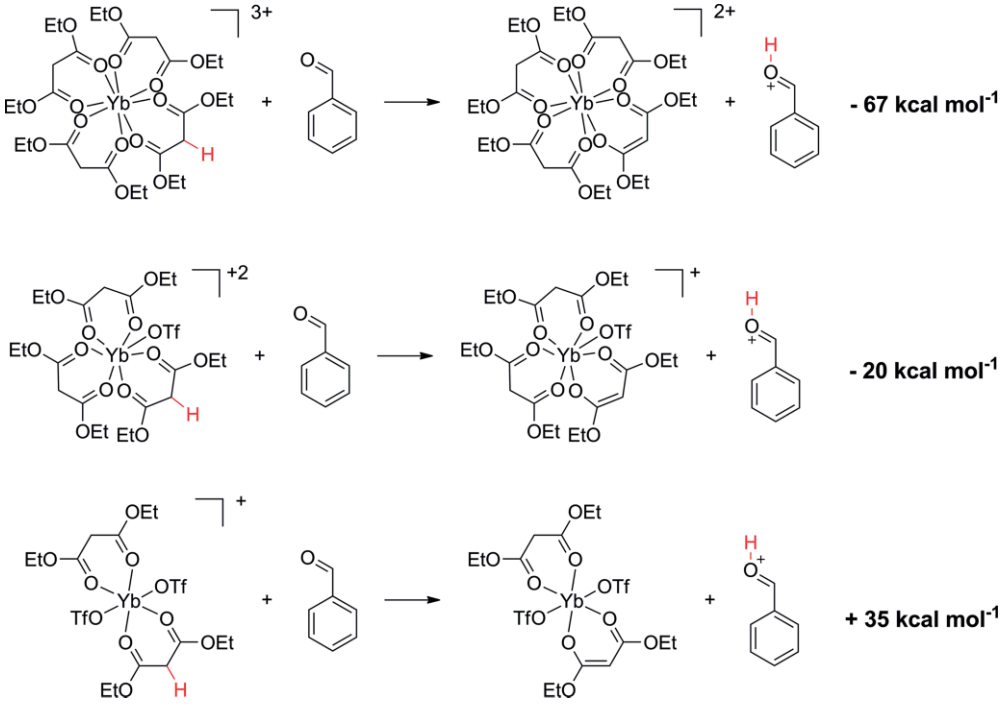

Scheme 2. B3LYP/6-311+G(d,p):SDD(Yb) reaction enthalpy for proton transfer between benzaldehyde and malonate in the triply, doubly and singly charged ytterbium complexes intercepted via ESI-MS monitoring.

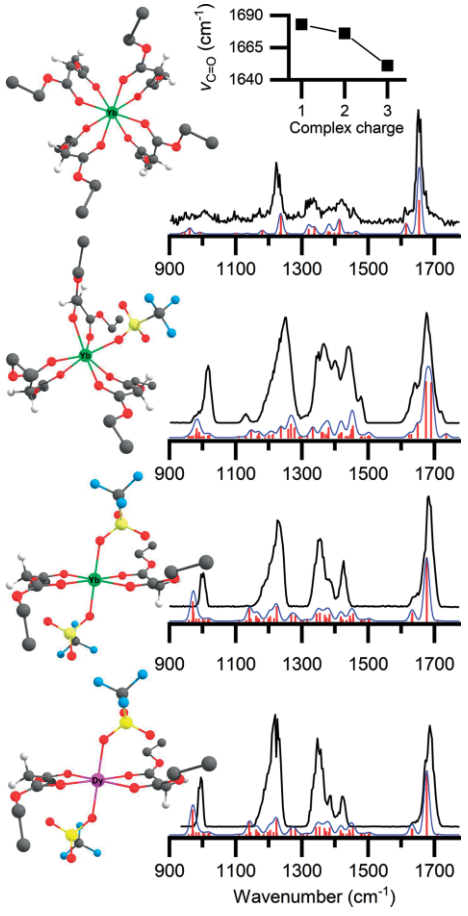

Figure 4. Vibrational spectra obtained for ytterbium complexes $[Yb(M)_4]^{3+}$, $[Yb(OTf)(M)_3]^{2+}$ and $[Yb(OTf)_2(M)_2]^{+}$ and for the dysprosium complex $[Dy(OTf)_2(M)_2]^{+}$. The IRMPD spectra are depicted by the black lines. The red bars represent the calculated intensities of the IR-active vibrational modes obtained by the DFT calculations and the theoretical Gaussian broadening bands are depicted in blue. The optimized geometry is depicted next to the spectrum. The hydrogen atoms of the ethyl groups were omitted for clarity. The oxygen atoms are red, sulfur is yellow, fluor is blue and carbon is grey. The inset graph above shows the correlation between the ytterbium complexes charge with the experimental vibrational frequency at the maximum of the carbonyl bands.

carbonyl C-O stretching modes. The bands are slightly red-shifted from the traditional ester carbonyl stretch (1750 cm^{-1}) due to the coordination to the Lewis acid. The red-shift can be directly correlated to the degree of carbonyl activation. The triply charged complex $[Yb(M)_4]^{3+}$ has $\nu_{C=O\ exp}$ = 1651 cm^{-1}; the doubly charged complex $[Yb(M)_3(Tf)]^{2+}$ $\nu_{C=O\ exp}$ = 1676 cm^{-1}; and the singly charged complex $[Yb(M)_2(Tf)_2]^{+}$ $\nu_{C=O\ exp}$ = 1683 cm^{-1} (see inset in Figure 4). The lower the wavenumber, the higher the carbonyl activation and thus the higher the reactivity of the malonate ester. This order of carbonyl activation determined in the gas phase is consistent with apparent reaction rates observed for the mechanistic routes **A**, **B** and **C** (Figure 2). Hence, IRMPD spectroscopy provides a direct information on the activation of malonate ligands within the lanthanide complexes.

Another effect that could be taken into account for the complexes reactivity is the coordination number. Note that the triply charged ion is the complex with higher coordination number (N_{coord} = 8), followed by the doubly charged (N_{coord} = 7) and the singly charged (N_{coord} = 6). We could expect that complexes of higher coordination number exhibit a longer Ln–O bond in order to minimize the steric hindrance between the ligands. A longer distance between the lanthanide and the basic site of the substrate should result in a less effective activation of the Lewis base. According to the DFT calculations, this longer distance does occur. The optimized structures reveal an average Yb–O bond length of 2.28 Å, 2.33 Å and 2.35 Å for the complexes $[Yb(M)_2(Tf)_2]^{+}$, $[Yb(M)_3(Tf)]^{2+}$ and $[Yb(M)_4]^{3+}$, respectively. However, this effect seems not to be as relevant as the complex charge state, since the lanthanide complex of higher N_{coord} exhibit the stronger carbonyl activation.

If we take into account the steric hindrance effect, we would also expect a shorter Ln–O distance in dysprosium complexes, since dysprosium exhibits a larger ionic radius than ytterbium. The DFT optimized structures however reveal the opposite. Dysprosium complexes display on average a Ln–O bond that is 0.04 Å longer than the Yb–O bond. This difference in bond length must occur therefore due to the higher electrophilicity of ytterbium, which also corroborates to the higher catalytic efficiency exhibited by the $Yb(OTf)_3$ salt.

Finally, the higher ytterbium electrophilicity must also correlate with a higher carbonyl activation, and the difference in carbonyl activation should be spectroscopically observed by a red shift of the carbonyl band of ytterbium complexes in comparison to dysprosium complexes. The $[Dy(OTf)_2(M)_2]^{+}$ has $\nu_{C=O\ exp}$ = 1686 cm^{-1}, 3 cm^{-1} blue-shifted in respect to the carbonyl band of the analogous ytterbium complex. These results indicate therefore a direct correlation between the carbonyl stretching of the activated substrate in gas phase and the catalytic efficiency of the Lewis acid in solution.

Conclusions

ESI-MS analysis of the reaction medium allowed us to identify a number of intermediates in a lanthanide triflate catalysed condensation reaction between diethyl malonate and benzaldehyde. Time dependent monitoring of the reaction mixture reveals different kinetic patterns associated with different charge-state lanthanide complexes, which indicates that the reaction proceeds faster within the complexes of higher charge state. The gas phase reactivity experiments evidenced a high reactivity of triply charged lanthanide complexes and these reactivities are also supported by DFT calculations. In addition, IRMPD spectroscopy revealed that a higher charge state of the lanthanide complexes correlates with a larger activation of the carbonyl group of the malonate ligands. The same method also showed larger substrate activation in ytterbium complexes than in analogous dysprosium complexes.

These results show that malonate activation in lanthanide complexes is predominantly driven by electrostatics. This is why anions largely affect the catalytic properties of the lanthanide complexes.[42–44] It explains why the use of poorly coordinating anions, such as triflates, is advantageous in lanthanide catalysis.

Experimental Section

Reaction monitoring with ESI(+)-MS

The reactions were performed in a 5 mL flask and the reactants were added in the following order: diethyl malonate (1.0 mmol), $Ln(OTf)_3$ (0.1 mmol) and benzaldehyde (1 mmol). Aliquots were periodically taken from the reaction medium, diluted to ca. 1×10^{-5} mol L^{-1} in acetonitrile and directly infused into the ESI source at a flow rate of 10 μL min^{-1}. The experiments were performed in a Q Exactive Orbitrap spectrometer. ESI parameters were as follow: spray voltage 3 kV, capillary temperature 300 °C, sheath gas 10, Probe heater temperature 30 °C and S-Lens RF Level 70 V.

Gas phase reactions

The experiments were performed with a quadrupole-octupole-quadrupole instrument TSQ 7000 equipped with an electrospray ionization (ESI) source. Solutions were introduced into the instrument via a fused-silica capillary. ESI parameters were as follow: spray voltage 4 kV, sheath gas pressure 70 psi, no auxiliary gas, capillary voltage 0 V, capillary temperature 250 °C and tube lens 140 V. The reactant ions were mass-selected by the first quadrupole and guided through the octopole collision cell. The pressure of the gas in the collision cell was measured by a baratron. The collision energy was set by the potential offset between the octopole and the ion source. The offset corresponding to zero collision energy was determined by retarding potential analysis.[45–47] The reactant as well as the product ions were mass-analysed by the second quadrupole and detected by a Daly-type detector.

Collision-induced dissociation (CID)

The CID experiments were performed in a Thermo Scientifc LTQ FT Ultra equipped with an electrospray source. The same aliquots used in the ESI(+)-MS reaction monitoring were used to generate the complex ions for the CID experiments. ESI parameters were follows: spray voltage 3 kV, capillary temperature 300 °C, S-Lens RF Level 70 V. The collisions were performed with helium gas using variable settings from 6 to 11 % of collision energy.

IRMPD Spectroscopy (CLIO)

IRMPD experiments were performed at a 7 T modified[48] Bruker APEX-Qe FT-ICR equipped with an electrospray (ESI) source located at the Centre de Laser Infrarouge d'Orsay in France.[49]

ESI parameters were as follow: Spray shield 4000 V, Capillary 4500 V, Capillary Exit 300 V, Deflector 280 V, Ion Funnel 1 150V, Ion Funnel 2 8V, Hexapole DC 5V, Trap –10V.

CLIO's Free Electron Laser tenable radiation in the 900 to 1800 cm^{-1} range was used to record frequency dependent photodissociation yields as reported in the literature.[48,50] The main photodissociation channel was the consecutive loss of Knoevenagel adducts or malonate ligands.

Theoretical calculations

Calculations were performed with the density functional theory method B3LYP with empirical dispersion corrections GD3-BJ. The basis set was a combination of the 6-311+G(d,p) basis set for C, H, O and F, the pc-2 basis set for S and the SDD basis set for the lanthanides, using 59 electrons in the effective core for ytterbium and 55 for dysprosium. All of the reported structures represent genuine minima on the respective potential energy surfaces, as confirmed by analysis of the corresponding Hessian matrices. All optimized structures and their energies are listed in the Supporting Information.

Acknowledgments

FAPESP (grants 2014/15962–5, 2015/08539–1) and CAPES (grant 23038.006960/2014–65). CLIO: Financial support from European Community's Horizon 2020 Programme (INFRAIA-01–2016, under Grant Agreement No. 730872), and the French FT-ICR network (FR3624CNRS) are gratefully acknowledged.

Keywords: Lewis acid catalysis · Lanthanide triflates · Reaction mechanisms · Structure elucidation · Reactive intermediates

[1] S. Kobayashi, C. Ogawa, *Chem. Eur. J.* **2006**, *12*, 5954–5960.
[2] M. Yamanaka, J. Itoh, K. Fuchibe, T. Akiyama, *J. Am. Chem. Soc.* **2007**, *129*, 6756–6764.
[3] W. G. Shou, Y. Y. Yang, Y. G. Wang, *Tetrahedron Lett.* **2006**, *47*, 1845–1847.
[4] A. Corma, H. García, *Chem. Rev.* **2003**, *103*, 4307–4365.
[5] G. K. Veits, J. Read De Alaniz, *Tetrahedron* **2012**, *68*, 2015–2026.
[6] S. Kobayashi, K. Manabe, *Pure Appl. Chem.* **2000**, *72*, 1373–1380.
[7] Y. Román-Leshkov, M. E. Davis, *ACS Catal.* **2011**, *1*, 1566–1580.
[8] A. Dzudza, T. J. Marks, *J. Org. Chem.* **2008**, *3*, 4004–4016.
[9] Q. Qian, W. Zhu, C. Lu, B. Zhao, Y. Yao, *Tetrahedron: Asymmetry* **2016**, *27*, 911–917.
[10] S. Kobayashi, I. Hachiya, T. Takahori, M. Araki, H. Ishitani, *Tetrahedron Lett.* **1992**, *33*, 6815–6818.
[11] S. Kobayashi, I. Hachiya, *J. Org. Chem.* **1994**, *59*, 3590–3596.
[12] Y. Liao, X. Liu, Y. Zhang, Y. Xu, Y. Xia, L. Lin, X. Feng, *Chem. Sci.* **2016**, *7*, 3775–3779.
[13] P. Muthuraja, S. Prakash, G. Siva, S. Muthusubramanian, P. Manisankar, *ChemistrySelect* **2017**, *2*, 10071–10075.
[14] I. M. de Oliveira, S. S. N. Vasconcelos, C. S. Barbeiro, T. C. Correra, A. Shamim, D. C. Pimenta, I. Caracelli, J. Zukerman-Schpector, H. A. Stefani, F. Manarin, *New J. Chem.* **2017**, *41*, 9884–9888.
[15] P. J. Tambade, Y. P. Patil, B. M. Bhanage, *Curr. Org. Chem.* **2009**, *13*, 1805–1819.
[16] R. Sakhuja, K. Pericherla, K. Bajaj, B. Khungar, A. Kumar, *Synthesis* **2016**, *48*, 4305–4346.
[17] H. Pellissier, *Coord. Chem. Rev.* **2017**, *336*, 96–151.
[18] X. Yan, R. M. Bain, Y. Li, R. Qiu, T. G. Flick, R. G. Cooks, *Org. Process Res. Dev.* **2016**, *20*, 940–947.
[19] J. Váňa, T. Terencio, V. Petrović, O. Tischler, Z. Novák, J. Roithová, *Organometallics* **2017**, *36*, 2072–2080.
[20] M. N. Godoi, F. de Azambuja, P. D. G. Martinez, N. H. Morgon, V. G. Santos, T. Regiani, D. Lesage, H. Dossmann, R. B. Cole, M. N. Eberlin, et al., *Eur. J. Org. Chem.* **2017**, *2017*, 1794–1803.
[21] T. Regiani, V. G. Santos, M. N. Godoi, B. G. Vaz, M. N. Eberlin, F. Coelho, *Chem. Commun.* **2011**, *47*, 6593–6595.
[22] C. Hinderling, C. Adlhart, P. Chen, *Angew. Chem. Int. Ed.* **1998**, *37*, 2685–2689; *Angew. Chem.* **1998**, *110*, 2831.
[23] P. Chen, *Angew. Chem. Int. Ed.* **2003**, *42*, 2832–2847; *Angew. Chem.* **2003**, *115*, 2938.
[24] S. A. McLuckey, J. M. Wells, *Chem. Rev.* **2001**, *101*, 571–606.
[25] M. Kolter, K. Böck, K. Karaghiosoff, K. Koszinowski, *Angew. Chem. Int. Ed.* **2017**, *56*, 13244–13248; *Angew. Chem.* **2017**, *129*, 13427.
[26] X. Yan, E. Sokol, X. Li, G. Li, S. Xu, R. G. Cooks, *Angew. Chem. Int. Ed.* **2014**, *53*, 5931–5935; *Angew. Chem.* **2014**, *126*, 6041.
[27] R. Galaverna, N. S. Camilo, M. N. Godoi, F. Coelho, M. N. Eberlin, *J. Org. Chem.* **2016**, *81*, 1089–1098.
[28] C. Iacobucci, S. Reale, F. De Angelis, *Angew. Chem. Int. Ed.* **2016**, *55*, 2980–2993; *Angew. Chem.* **2016**, *128*, 3032.
[29] L. S. Santos, *Eur. J. Org. Chem.* **2008**, 235–253.
[30] F. Coelho, M. N. Eberlin, *Angew. Chem. Int. Ed.* **2011**, *50*, 5261–5263; *Angew. Chem.* **2011**, *123*, 5370.
[31] P. K. Sarkar, P. K. Prajapati, V. J. Shukla, B. Ravishankar, A. K. Choudhary, *Indian J. Exp. Biol.* **2009**, *47*, 987–992.
[32] L. Jašíková, M. Anania, S. Hybelbauerová, J. Roithová, *J. Am. Chem. Soc.* **2015**, *137*, 13647–13657.

[33] J. Jašík, J. Žabka, J. Roithová, D. Gerlich, *Int. J. Mass Spectrom.* **2013**, *354–355*, 204–210.
[34] J. Roithová, Š. Janková, L. Jašíková, J. Váňa, S. Hybelbauerová, *Angew. Chem. Int. Ed.* **2012**, *51*, 8378–8382; *Angew. Chem.* **2012**, *124*, 8503.
[35] J. Schulz, L. Jašíková, A. Škríba, J. Roithová, *J. Am. Chem. Soc.* **2014**, *136*, 11513–11523.
[36] J. Roithová, *Chem. Soc. Rev.* **2012**, *41*, 547.
[37] L. Jašíková, J. Roithová, *Chem. Eur. J.* **2018**, *24*, 3374–3390.
[38] H. Tsuruta, K. Yamaguchi, T. Imamoto, *Tetrahedron* **2003**, *59*, 10419–10437.
[39] P. B. Armentrout, *Int. J. Mass Spectrom.* **2000**, *200*, 219–241.
[40] J. Roithová, *Pure Appl. Chem.* **2011**, *83*, 1499–1506.
[41] S. Colette, B. Amekraz, C. Madic, L. Berthon, G. Cote, C. Moulin, *Inorg. Chem.* **2003**, *42*, 2215–2226.
[42] N. R. Champness, *Dalton Trans.* **2011**, *40*, 10311–10315.
[43] W. Beck, K. Sünkel, *Chem. Rev.* **1988**, *88*, 1405–1421.
[44] J. H. Kim, J. W. Lee, U. S. Shin, J. Y. Lee, S. Lee, C. E. Song, *Chem. Commun.* **2007**, 4683.
[45] L. Ducháčková, J. Roithová, *Chem. Eur. J.* **2009**, *15*, 13399–13405.
[46] E. Andris, R. Navrátil, J. Jašík, T. Terencio, M. Srnec, M. Costas, J. Roithová, *J. Am. Chem. Soc.* **2017**, *139*, 2757–2765.
[47] P. B. Armentrout, *J. Am. Soc. Mass Spectrom.* **2002**, *13*, 419–434.
[48] J. M. Bakker, T. Besson, J. Lemaire, D. Scuderi, P. Maître, *J. Phys. Chem. A* **2007**, *111*, 13415–13424.
[49] R. Prazeres, F. Glotin, C. Insa, D. A. Jaroszynski, J. M. Ortega, *Eur. Phys. J. D* **1998**, *3*, 87–93.
[50] F. Lanucara, B. Chiavarino, D. Scuderi, P. Maitre, S. Fornarini, M. E. Crestoni, *Chem. Commun.* **2014**, *50*, 3845–3848.

Received: January 31, 2019